の簡略化を図る.

C. 結果と考察

[電流源内蔵型マイクロチップ]

受光機能だけでなく同時多点刺激機能，刺激電流生成機能を搭載した新世代の人工視覚デバイス(AR39)の試作を行った．図 3 に試作デバイスのチップ写真，図 4 にマイクロチップのブロック図を示す．マイクロチップはサイズを 200 μm 角に縮小し，電極数は 1 極という構成で，VDD･GND の電源入力，電極選択のためのディジタル入力である CONT1･CONT2，外部からの刺激電流を入力する STIM の計 5 本の制御配線によって動作する．

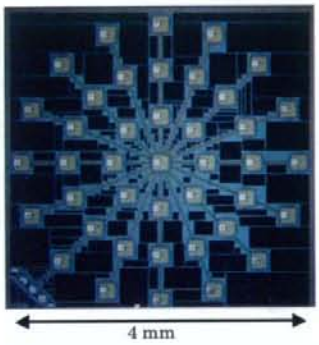


図 3：電流源内蔵型マイクロチップアレイ写真

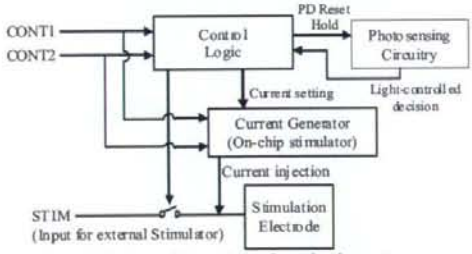


図 4：マイクロチップ回路ブロック

チップ内には制御回路，受光回路，刺激電流生成回路を搭載している．チップの動作フェーズの指定を行う CONT1 とチップの動作条件を指定する CONT2 の 2 本の配線より分散配置された複数のユニットチップを任意に選択でき同時多点刺激を実現する．内部供給の刺激電流は 50 μA~1000 μA まで 50 μA ステップで指定可能で，STIM を用いた外部供給に切り替えることも可能である．そして，機能評価を行い従来デバイスの動作に付け加え，同時多点刺激および刺激信号の内部生成が可能なことを確認した．

[動物実験による機能評価]

大阪大学医学部の協力のもと，試作したデバイスをウサギ眼球に埋植し，光応答による網膜の電気刺激実験を行った．実験に使用したウサギは変性ではない普通のウサギのため，光応答の照射光は可視光ではなく近赤外光を用いた．また，視覚再生に有効な刺激が行われているか確認するため，頭部に挿入した電極により脳波の測定を行い，網膜を電気刺激したことによって脳内に誘発される電位(EEP; Electrical Evoked Potential)の検出に成功した．図 5 の 4 つの波形はそれぞれ上から刺激電極選択パルス入力時，刺激出力時共に赤外光を照射，パルス入力時のみ赤外光を照射，刺激出力時のみ赤外光を照射，赤外光を照射しなかった場合に脳波を測定したものである．刺激電極選択パルス入力時に赤外光を照射した場合のみ刺激電流が出力されており，EEP 波形が観測された．

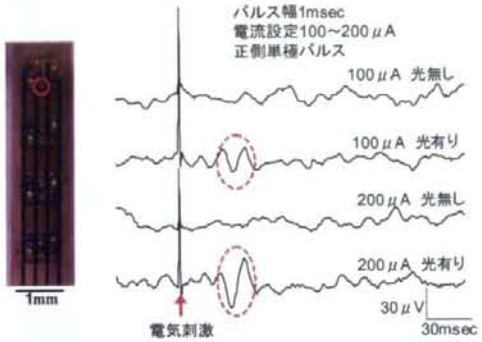


図 5：兎眼球埋植デバイスによる EEP

[LSI メタル配線によるマイクロチップ間接続]

これまでのデバイスでは全ての単位チップに信号入力用の配線接続を必要としていた．そこで，単位チップ同士をあらかじめ LSI メタル配線層によって接続し，あとからメタル配線層を残して単位チップに分割することで，LSI メタル配線層を単位チップ間にフレキシブルな配線として用いるデバイスの実装を行った(図 6)．

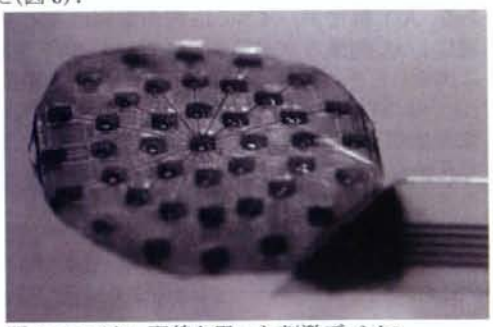

図 6:LSI メタル配線を用いた刺激デバイス

D. 結論

LSI による分散型人工視覚デバイスを網膜下へ適用するために光応答型マイクロチップの開発を行った．さらに試作したデバイスを用いてウサギ *in vivo* 電気刺激実験を行い，光照射下のみに EEP 波形を検出

することを確認し，光応答に対する有効的な刺激が行われたことを実証した．また LSI メタル配線層を利用したマイクロチップ間接続方式を開発した．今後，種々の動物実験を行うと共に，実装の信頼性向上を図る必要がある．

E. 健康危険情報
なし．

F. 研究発表
1．論文発表
T. Tokuda; R. Asano; S. Sugitani; M. Taniyama; Y. Terasawa; M. Nunoshita; K. Nakauchi; T. Fujikado; Y. Tano; **J. Ohta**, "Retinal stimulation on rabbit using CMOS-based multi-chip flexible stimulator toward retinal prosthesis," Jpn. J. Appl. Phys. **47** (4), 3220-3225, 2008.
Y. Terasawa, A. Uehara, E. Yonezawa, T. Saitoh., K. Shodo, M. Ozawa, Y. Tano, **J. Ohta**, "A Visual Prosthesis with 100 Electrodes Featuring Wireless Signals and Wireless Power Transmission," IEICE Electronics Express (ELEX), **5** (15), 574-580, 2008.

2．総説・著書
太田 淳，「人工視覚デバイス」，映情学会誌，**62** (6), pp. 827-831, 2008.

3．学会発表
T. Tokuda, R. Asano, Y. Terasawa, M. Nunoshita, K. Nakauchi, K. Nishida, Y. Kitaguchi, T. Fujikado, Y. Tano, J. Ohta, "Stimulation on rabbit retina using CMOS LSI-based flexible stimulator for retinal prosthesis," Int'l Symposium Biological and Physiological Engineering, The 22nd SICE Symposium on Biological and Physiological Engineering (ISBPE / 22nd BPES), 2008/1/14, Songhuajiang Gloria Plaza Hotel Harbin, China
T. Tokuda, R. Asano, Y. Terasawa, Y. Tano, J. Ohta, "A Microelectronics-Based Flexible Retinal Stimulator for Retinal Prosthesis With an Improved Safety and Fault Tolerance," ARVO Annual Meeting, 2008/4/28, Fort Lauderdale, FL.
J. Ohta, "Retinal Implants," IEEE Int'l Solid-State Circuits Conference (ISSCC), 2009/2/8, San Franscico Mrriott Hotel.

G. 知的財産権の出願・登録状況
1．特許出願
なし

研究成果の刊行に関する一覧表


1. **Kondo M**, Sakai T, et al. Generation of a transgenic rabbit model of retinal degeneration. Invest Ophthalmol Vis Sci. 2009 Mar;50(3):1371-7.

2. Sugita S, **Kondo M**, et al. Correlation between macular volume and focal macular electroretinogram in patients with retinitis pigmentosa. Invest Ophthalmol Vis Sci. 2008;49:3551-3558.

3. **Kondo M**, Kurimoto Y, et al. Recording focal macular photopic negative response (PhNR) from monkeys. Invest Ophthalmol Vis Sci. 2008;49:3544-50.

4. T. Tokuda; R. Asano; S. Sugitani; M. Taniyama; Y. Terasawa; M. Nunoshita; K. Nakauchi; T. Fujikado; Y. Tano; **J. Ohta**, "Retinal stimulation on rabbit using CMOS-based multi-chip flexible stimulator toward retinal prosthesis," Jpn. J. Appl. Phys. **47** (4), 3220-3225, 2008.

5. Y. Terasawa, A. Uehara, E. Yonezawa, T. Saitoh., K. Shodo, M. Ozawa, Y. Tano, **J. Ohta**, "A Visual Prosthesis with 100 Electrodes Featuring Wireless Signals and Wireless Power Transmission," IEICE Electronics Express (ELEX), **5** (15), 574-580, 2008.

6. Sato T, **Fujikado T**, Lee TS, Tano Y. Direct Effect of Electrical Stimulation on Induction of Brain-derived Neurotrophic Factor from Cultured Retinal Mueller Cells. Invest Ophthalmol Vis Sci. 2008;49:4641-6.

7. Kitaguchi Y, **Fujikado T**, Bessho K, Sakaguchi H, Gomi F, Yamaguchi T, Nakazawa N, Mihashi T, **Tano Y**. Adaptive Optics Fundus Camera to Examine Localized Changes in Photoreceptor Layer of Fovea, Ophthalmology, 2008; 115: 1771-1777

8. Bessho K, **Fujikado T**, Mihashi T, Yamaguchi T, Nakazawa N, Tano Y Photoreceptor images of normal eyes and of eyes with macular dystrophy obtained in vivo with an adaptive optics fundus camera J J OPHTHALMOL 2008: 52;380-385

9. Kobayashi I, **Hirakata A**, et al.Vitreous surgery for macular hole in patients with Vogt-Koyanagi-Harada disease. Clin. Experiment.Ophthalmol,. 2008;36;861-864,

10. Y. Terasawa, M. Ozawa, T. Tokuda, J. Ohta and Y. Tano Large-Surface-Area Electrodes Based on Bulk Micromachining, Investigative Ophthalmology and Visual Science, Vol.49(5), p. S3020, 2008

11. Y. Terasawa, M. Ozawa, J. Ohta and Y. Tano, Bulk Micromachining-based Multielectrode Array for Retinal Prostheses, The Eye and The Chip 2008 World Congress, Detroit, June 14, 2008

12. 寺澤靖雄, 小澤素生, 田代洋行, 太田 淳, 田野保雄, 人工視覚システムにおけるバルク材料を用いた高信頼性刺激電極の開発, 人工臓器, Vol.37, No.2, p. S-180, 2008

13. Okazaki Y, Morimoto T, Sawai H. Parameters of optic nerve electrical stimulation affecting neuroprotection of axotomized retinal ganglion cells in adult rats. Neurosci Res. 61(2):129-35, 2008.

14. 太田 淳, 「人工視覚デバイス」, 映情学会誌, **62** (6), pp. 827-831, 2008.

15. 平形明人：網膜上組織からの情報. 日本の眼科 78：589-593, 2008

16. Taki, **Hirakata A**, Ohira: Macular edema from distant branch retinal vein occlusion subsiding after vitrectomy. Jpn J Ophthalmol 2009 Mar-Apr;53(2):184-6.

17. Futagami S, Inoue M, **Hirakata A**: Removal of internal limiting membrane for recurrent myopic traction maculopathy. Clinical Experimental Ophthalmology. 2008 36(8):782-5

18. Keino H, Watanabe T, et al:Therapeutic effect of the potent IL-12/IL-23 inhibitors STA-5326 on experimental autoimmune uveoretinitis. Arthritis Research & Therapy 10:122, 2008

19. Kawasaki R, Wang JJ, Ji GJ, Taylor B, Oizumi T, Daimon M, Kato T, Kawata S, Kayama T, **Tano Y**, Mitchell P, Yamashita H, Wong TY. Prevalence and risk factors for age-related macular degeneration in an adult Japanese population: the Funagata study. Ophthalmology. 2008 Aug;115(8):1376-81

20. Sayanagi K, Ikuno Y, Soga K, **Tano Y**. Photoreceptor inner and outer segment defects in myopic foveoschisis. Am J Ophthalmol. 2008 May;145(5):902-8.

21. Sawa M, Gomi F, Ohji M, Tsujikawa M, Fujikado T, **Tano Y**. Fundus autofluorescence after full macular translocation surgery for myopic choroidal neovascularization. Graefes Arch Clin Exp Ophthalmol. 2008 Aug;246(8):1087-95.

22. Koyama Y, Matsuzaki S, Gomi F, Yamada K, Katayama T, Sato K, Kumada T, Fukuda A, Matsuda S, **Tano Y**, Tohyama M. Induction of amyloid beta accumulation by ER calcium disruption and resultant upregulation of angiogenic factors in ARPE19 cells. Invest Ophthalmol Vis Sci. 2008 Jun;49(6):2376-83.

23. Fang X, Sakaguchi H, Gomi F, Oshima Y, Sawa M, Tsujikawa M, Ikuno Y, Kamei M, Kusaka S, **Tano Y**. Efficacy and safety of one intravitreal injection of bevacizumab in diabetic macular oedema. Acta Ophthalmol. 2008 Nov;86(7):800-5.

24. Kasai A, Shintani N, Kato H, Matsuda S, Gomi F, Haba R, Hashimoto H, Kakuda M, **Tano Y**, Baba A. Retardation of retinal vascular development in apelin-deficient mice. Arterioscler Thromb Vasc Biol. 2008 Oct;28(10):1717-22.

25. Sawa M, Gomi F, Tsujikawa M, Ikuno Y, Sakaguchi H, Sayanagi K, **Tano Y**. Abnormal fundus autofluorescence patterns in myopic choroidal neovascularisation. Br J Ophthalmol. 2008 Sep;92(9):1236-40.

26. Sato S, Omori Y, Katoh K, Kondo M, Kanagawa M, Miyata K, Funabiki K, Koyasu T, Kajimura N, Miyoshi T, Sawai H, Kobayashi K, Tani A, Toda T, Usukura J, Tano Y, **Fujikado T**, Furukawa T. Pikachurin, a dystroglycan ligand, is essential for photoreceptor ribbon synapse formation. Nat Neurosci. 2008 Aug;11(8):923-31.

27. Sato T, **Fujikado T**, Morimoto T, Matsushita K, Harada T, Tano Y. Effect of electrical stimulation on IGF-1 transcription by L-type calcium channels in cultured retinal Müller cells. Jpn J Ophthalmol. 2008 May-Jun;52(3):217-23.

28. **Tano Y**; Pegaptanib Sodium Multi-center Study Group. [Pegaptanib sodium one-year treatment study for neovascular age-related macular degeneration]. Nippon Ganka Gakkai Zasshi. 2008 Jul;112(7):590-600.

tapraid4/z7g-iovs/z7g-iovs/z7g00309/z7g9560d09a | moyerr | S=12 | 12/30/08 | 16:42 | Art: 08-2863 | Input-mr

# Generation of a Transgenic Rabbit Model of Retinal Degeneration

*Mineo Kondo,[1] Takao Sakai,[1] Keiichi Komeima,[1] Yukihide Kurimoto,[1] Shinji Ueno,[1] Yuji Nishizawa,[2] Jiro Usukura,[3] Takashi Fujikado,[4] Yasuo Tano,[5] and Hiroko Terasaki[1]*

**Purpose.** To generate a transgenic (Tg) rabbit model of retinal degeneration and to characterize the pattern of degeneration by using histology and electrophysiology.

**Methods.** Rhodopsin Pro347Leu Tg rabbits were generated by BAC transgenesis. Tg rabbits were identified by Southern blot analysis, and the expression levels were measured by quantitative RT-PCR. Retinal histology was examined by light and electron microscopy and immunohistochemistry. Retinal function was assessed by full-field electroretinograms (ERGs).

**Results.** Six lines of Tg rabbits were generated, and two lines with higher levels of expression showed rod-dominant progressive retinal degeneration. Retinal histology indicated a marked regional variation in the loss of photoreceptors with the central retina more severely affected than the peripheral retina. The characteristics of the ERGs of transgenic rabbits indicated that the rod components of the ERGs were reduced to only 5% by 48 weeks, whereas the cone components remained at 35% in the wild-type at the same time point. The retinal ultrastructure of Tg rabbits showed a large number of small vesicles that accumulated in the extracellular space of the photoreceptors.

**Conclusions.** To the best of the authors' knowledge, this is the first rabbit model of progressive retinal degeneration. Because rabbits have large eyes and are easy to handle and breed, they will provide a useful animal model for the study of the pathophysiology of and new treatments for retinal degeneration. (*Invest Ophthalmol Vis Sci.* 2009;50:000–000) DOI:10.1167/iovs.08-2863

AQ: 1

Retinitis pigmentosa (RP) is the name given to a group of inherited retinal disorders characterized by a progressive loss of rod and cone photoreceptors and eventual atrophy of the entire retina.[1–3] The worldwide prevalence of RP is approximately 1 in 4000, meaning that more than 1 million individuals are affected worldwide.[3] RP is genetically heterogeneous; mutations in several photoreceptor-specific and some nonspecific genes are known to cause the condition.[4] Of these, mutations in the rhodopsin gene are the most prevalent class identified to date, causing approximately 25% to 40% of the autosomal dominant RP cases.[5,6]

Animal models of RP are important for understanding the pathophysiology and for developing new treatments for these diseases. Various naturally occurring and genetically manipulated animal models of RP have been studied—for example, fruit flies, zebrafish, chickens, mice, rats, cats, dogs, and pigs (for reviews, see Refs. 7, 8). Of these models, midsized and large animal models have become particularly important because their large eyes make it easier to test new treatments. These treatments may include surgical procedures such as intraocular devices,[9,10] subretinal injection of genes for gene therapy,[11] and implantation of retinal prostheses.[12] Several models of retinal degeneration have been identified or generated in cats,[13,14] dogs,[15,16] and pigs,[17] and colonies of affected animals have been established. However, a rabbit model of progressive retinal degeneration has not yet been produced, despite the fact that this animal has large eyes and is easy to breed and handle. In addition, there is a considerable accumulation in the anatomy and physiology of the rabbit eye.[18–21]

AQ: 2

Recent advances in the use of bacterial artificial chromosomes (BACs) modified by homologous recombination have promoted the use of this powerful tool in the generation of transgenic (Tg) animals because this technique makes possible the precise and efficient engineering of large DNA fragments.[22–25] In the present study, we used BAC transgenesis to generate a rhodopsin Tg rabbit model of retinal degeneration. These Tg rabbits exhibited rod-dominant, progressive photoreceptor degeneration and striking regional variation in the pattern of photoreceptor loss.

## Methods

This study was conducted in accordance with the ARVO Statement for the Use of Animals in Ophthalmic and Vision Research. All protocols were approved by the Institutional Review Board of the Nagoya University Graduate School of Medicine.

### Rabbit Rhodopsin BAC Clone

The rabbit rhodopsin BAC clone, LB1-7M22, was selected from the LBNL-1 New Zealand White Rabbit BAC library by hybridization of high-density arrayed nylon filters using a probe that consisted of a [$P^{32}$]-labeled fragment of exon 5 of the rabbit rhodopsin gene. The clone was obtained from the BACPAC Resources Center at the Children's Hospital of Oakland Research Institute. The presence of a full-length rabbit rhodopsin genomic sequence was verified by Southern blot analysis with a probe that consisted not only of exon 4 of the rhodopsin gene but also exon 14 of the rabbit *WDR10* gene and exon 25 of the rabbit *PLXND1* gene. These latter two genes are the 5′- and 3′-flanking genes, respectively, of the rabbit rhodopsin gene (Fig. 1A). The exon 4 genomic fragment of the rabbit rhodopsin gene, exon 14 of the rabbit *WDR10* gene, and exon 25 of the rabbit *PLXND1* gene

F1

From the [1]Department of Ophthalmology, Graduate School of Medicine, and the [3]Department of Materials Physics and Engineering, Graduate School of Engineering, Nagoya University, Nagoya, Japan; the [2]Research Institute of Life and Health Sciences, Chubu University, Kasugai, Japan; and the Departments of [4]Applied Visual Science and [5]Ophthalmology, Graduate School of Medicine, Osaka University, Suita, Japan.

Supported by Health Sciences Research Grant H16-sensory-001 from the Ministry of Health, Labor, and Welfare of Japan, and Grants 18591913 and 18390466 from the Ministry of Education, Culture, Science, and Technology of Japan.

Submitted for publication September 12, 2008; revised November 9, 2008; accepted Month Day, 2008.

Disclosure: **M. Kondo**, None; **T. Sakai**, None; **K. Komeima**, None; **Y. Kurimoto**, None; **S. Ueno**, None; **Y. Nishizawa**, None; **J. Usukura**, None; **T. Fujikado**, None; **Y. Tano**, None; **H. Terasaki**, None

The publication costs of this article were defrayed in part by page charge payment. This article must therefore be marked "*advertisement*" in accordance with 18 U.S.C. §1734 solely to indicate this fact.

Corresponding author: Mineo Kondo, Department of Ophthalmology, Nagoya University Graduate School of Medicine, 65 Tsuruma-cho, Showa-ku, Nagoya 466-8550, Japan; kondomi@med.nagoya-u.ac.jp.






ARTICLE TYPE: **RETI**

tapraid4/z7g-iovs/z7g-iovs/z7g00309/z7g9560d09a | moyerr | S=12 | 12/30/08 | 16:42 | Art: 08-2863 | Input-mr



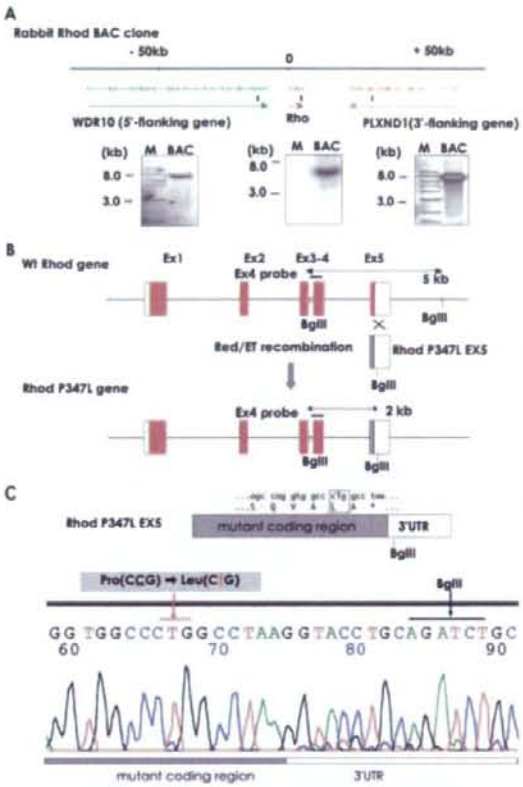


COLOR

FIGURE 1. Rhodopsin P347L BAC construction by recombineering. (**A**) Presumed structure of the rabbit rhodopsin BAC clone. The BAC clone contains the full-length rabbit rhodopsin genomic sequence, as determined by Southern hybridization probed by the 5′-flanking gene (*left*), rhodopsin gene (*middle*), and 3′-flanking gene (*right*). *Underbars*: positions of the Southern hybridization probes used. (**B**) The transgene construct. The sequence of exon 5 of the WT rhodopsin gene (*top*) was replaced by the rhodopsin P347L exon 5 sequence (*middle*) by Red/ET recombination. The rhodopsin P347L gene (*bottom*) has a *Bgl*II restriction site for Tg. (**C**) Sequence analysis for the rhodopsin P347L mutation. The rhodopsin P347L exon 5 fragment was amplified from the rhodopsin P347L BAC construct by PCR and sequenced.

were amplified by PCR and subcloned into the pGEM-T easy vector (Promega, Madison, WI) for labeling with [$P^{32}$].

## BAC Transgenic Construct

A rhodopsin P347L BAC Tg construct harboring a C-to-T transition in exon 5 of the rabbit rhodopsin gene was generated by BAC recombineering (Fig. 1B). A point mutation was introduced into the rabbit rhodopsin BAC clone (Red/ET Counter Selection BAC Modification Kit; Gene Bridges, Heidelberg, Germany).[24] In brief, an rpsL-neo counter selection cassette, flanked by 40-nucleotide homologous arm sequences on either side of the C-to-T transition site of the rhodopsin gene, was amplified by PCR. The amplified rpsL-neo counter selection cassette was inserted into the rhodopsin gene of the rabbit BAC clone by Red/ET recombination. The subcloned exon 5 fragment of the rabbit rhodopsin gene was modified with a C-to-T transition at proline 347, and the serial restriction sites *Kpn*I, *Pst*I, and *Bgl*II in the 3′-untranslated region. The modified sequence was subcloned into the pGEM-T easy vector for sequencing. The rpsL-neo cassette inserted into the rhodopsin gene of the rabbit BAC clone was replaced by the modified exon 5 fragment by using rpsL counter selection. The BAC modification was verified by Southern blot analysis (Fig. 1A) and sequencing (Fig. 1C). The rhodopsin P347L BAC transgene was purified in a modified procedure.[26] The BAC Tg construct was extracted from 250 mL of *Escherichia coli* culture (Nucleobond Plasmid Purification kit; Macherey-Nagel, Düren, Germany). For purification, 10 μg of the BAC Tg construct was linearized overnight with PI-*Sce*I endonuclease (New England Biolabs, Beverly, MA), which cleaves a unique site in the BACe3.6 vector sequence. The linearized BAC DNA was separated by pulsed-field gel electrophoresis (PFGE) and extracted from the preparative pulsed-field gel by electroelution. After dialysis against a TE buffer containing 0.1 mM EDTA, aliquots of DNA were subjected to PFGE for size and quality control. The BAC DNA concentration was adjusted to 1 ng/μL for microinjections. The aliquots of BAC DNA solution were stored at 4°C until the microinjections were performed.

## Rhodopsin P347L Transgenic Rabbits

Rhodopsin P347L Tg rabbits were generated by pronuclear injection of the BAC Tg construct into New Zealand White rabbit embryos. Transgenic founders and germline transmission of the BAC Tg construct were assessed by Southern blot analysis of *Bgl*II-digested ear DNA, which was probed with a [$P^{32}$]-labeled exon 4 fragment of the rabbit rhodopsin gene.

## DNA Fluorescence In Situ Hybridization Analysis

DNA FISH analysis was used to examine the actual site of the integrated transgene for each Tg line. Chromosome preparations were obtained with standard techniques and hybridized with a full-length rhodopsin P347L BAC Tg construct as a probe. The probe was labeled with biotin (Roche Diagnostics GmbH, Mannheim, Germany) and detected with avidin-FITC (Fluorescein Avidin D; Vector Labs, Burlingame, CA). The site of the transgene integration was determined by using a standard rabbit chromosome map.[27]

## Quantitative RT-PCR

One milligram of total retinal RNA (12 weeks of age) was incubated with 200 units of reverse transcriptase (SuperScript II; Invitrogen, Carlsbad, CA), and the cDNA was used for quantitative RT-PCR (qRT-PCR; QuantiTect SYBR Green PCR Kit; Qiagen, Valencia, CA) and a thermocycler (LightCycler 1.5; Roche Applied Science, Indianapolis, IN). Twenty-microliter reactions were loaded into the thermocycler containing 2 μL of the cDNA sample and 0.5 μM of primers specific for the mutated rhodopsin (forward: 5′-CTA CAT CAT GAT GAA CAA GCA G-3′ and reverse: 5′-TGG CTG GTC TCC GTC TTG GAA-3′) or common primers for wild-type (WT) and mutated rhodopsin (forward: 5′-CTA CAT CAT GAT GAA CAA GCA G-3′ and reverse: 5′-GCA GTG CAG ATC TGC AGG T-3′). For quantification, a standard curve was generated from a cDNA template for each gene. The relative levels of transgene expression were quantified as a ratio of the Tg to the endogenous rhodopsin mRNA.

## Clinical Ophthalmic Observations

Ophthalmic examinations were conducted every month after birth. Examinations of the cornea, anterior chamber, iris, and lens were performed by slit-lamp biomicroscopy. The vitreous and retina were examined by indirect ophthalmoscopy. A fundus camera (Kowa, Nagoya, Japan) was used for fundus photography and fluorescein angiography.

## Electroretinograms

Animals were dark-adapted for 60 minutes, then anesthetized with ketamine (25 mg/kg, IM) and xylazine (2 mg/kg, IM). ERGs were recorded with Burian-Allen bipolar contact lens electrodes (Hansen

tapraid4/z7g-iovs/z7g-iovs/z7g00309/z7g9560d09a | moyerr | S=12 | 12/30/08 | 16:42 | Art: 08-2863 | Input-mr



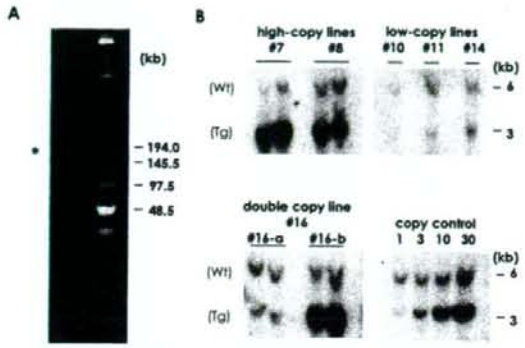


**FIGURE 2.** Generation of rhodopsin P347L Tg rabbits. (A) Purified rhodopsin P347L transgene construct. PFGE showed that the purified rhodopsin P347L transgene construct was almost 150 kb in size. (B) Southern blot analysis of F1 rabbits of rhodopsin P347L Tg lines. The endogenous rhodopsin WT gene and the rhodopsin P347L transgene were detected as 6 and 3 kb *Bgl*II fragments that hybridized to an exon 4 probe. The copy numbers of the integrated transgene for each line were determined by comparing with a control copy number signal intensity.

Laboratory, Iowa City, IA). The animals were placed in a Ganzfeld bowl and stimulated with stroboscopic stimuli of 2.2 log cd · s · $m^{-2}$ (photopic units) maximum intensity. Eight steps of stimulus intensities, ranging from −4.8 to 2.2 log cd · s · $m^{-2}$, were used for the scotopic ERG recordings, and four steps of stimuli, ranging from −0.8 to 2.2 log cd · s · $m^{-2}$, were used for the photopic ERGs. The photopic ERGs were recorded on a rod-suppressing white background of 1.3 log cd · $m^{-2}$. The signals were amplified, bandpass filtered between 0.3 and 1000 Hz, and averaged by a computer-assisted signal analysis system (MEB-9100 Neuropack; Nihon Kohden, Tokyo, Japan). The electrical activities of the rod and cone photoreceptors were assessed by the maximum response of the rod and cone a-waves. The maximum rod a-wave was extracted by waveform subtraction of the photopic ERG from the scotopic ERG at the maximum stimulus intensity of 2.2 log cd · s · $m^{-2}$.

Rod and cone photoreceptor function was also assessed by the a-wave (P3)-fitting model of Hood and Birch.[28] The a-wave was fitted with the following equation:

$$P3(t, t) = \{1 - \exp[-t \cdot S(t - t_d)^2]\} \cdot Rm(\text{for } t > t_d)$$

where $t$ is the flash energy (log cd · s · $m^{-2}$); $t_d$ is the time delay, $t$ is the time after the flash onset, $S$ is the sensitivity, and $Rm$ is maximum response amplitude.

## Retinal Histology

Rabbit eyes were fixed overnight in a mixture of 10% neutral buffered formalin and 2.5% glutaraldehyde; F-G fixative), then transferred to 10% neutral buffered formalin. The tissues were trimmed, embedded in paraffin, sectioned vertically through the optic nerve (superior-inferior), and stained with hematoxylin and eosin. The thickness of the outer nuclear layer (ONL) was measured at 10 locations at 2-mm intervals.

## Immunohistochemistry

Freshly prepared rabbit eyes were fixed with 4% formaldehyde in phosphate buffer for 2 hours at 4°C. After fixation, the eyes were immersed in 20% sucrose, frozen in OCT compound (Sakura Finetechnical Co., Ltd., Tokyo, Japan), and sectioned at 15 μm. The tissue sections were processed for immunofluorescence staining with anti-rhodopsin antibody (RET-P1; Santa Cruz Biotechnology), followed by Alexa Fluor 488–conjugated anti-mouse IgG and Alexa Fluor 568–conjugated peanut agglutinin (PNA; Invitrogen), a lectin that binds specifically to rabbit cone photoreceptors.[29] Specimens were observed with a fluorescence microscope (BX61 microscope with digital photograph system DP70-BSW; Olympus, Tokyo, Japan).

## Electron Microscopy

Eyes were enucleated from anesthetized rabbits (6-week-old WT and line 7 Tg rabbits). The anterior segment was removed, and the retina was fixed in 2.5% glutaraldehyde for 2 hours. After subsequent fixation in 1% osmium tetroxide for 90 minutes, the retina was dehydrated through a graded series of ethanols (50%–100%), and cleared in propylene oxide. Finally, the tissue was embedded in epoxy resin. Ultrathin sections were cut on an ultramicrotome (Ultracut E; Reichert-Jung, Vienna, Austria) and stained with uranyl acetate and lead citrate. The stained sections were observed by transmission electron microscopy (H-7650; Hitachi Co., Tokyo, Japan).

# RESULTS

## Generation of Transgenic Rabbits

We identified a rabbit rhodopsin BAC clone that included sequences approximately 150 kb upstream of the transcription initiation codon, the entire rhodopsin structural gene, and sequences downstream of the termination codon of the gene (Fig. 1A). Assuming that these genomic sequences would lead to correct expression of the rhodopsin gene, we inserted a C-to-T transition into the BAC clone in the codon of proline 347 by using BAC recombineering (Fig. 1B). The mutation introduced into the BAC Tg construct was then confirmed by sequence analysis (Fig. 1C). The C-to-T transition in exon 5 of the rabbit rhodopsin gene locus resulted in a proline-to-leucine substitution at codon 347.

After the BAC modification in *E. coli*, the linearized BAC Tg construct was purified and injected into rabbit embryos at the pronucleus stage. PFGE showed that the purified rhodopsin P347L Tg construct was approximately 150 kb (Fig. 2A). Southern blot analysis showed that 12 of 80 newborn rabbits (15%) were transgene positive, and 10 of the 12 survived (Table 1). These 10 founders were bred with WT rabbits, and six founders transmitted the transgene to their offspring. F2 T1

## Characteristics of Each Line of Transgenic Rabbit

FISH analysis showed that five founders, rabbits 7, 8, 10, 11, and 14, had a single site of transgene integration, and one founder, rabbit 16, had integrations at two sites (Table 2). Three lines, 10, 11, and 14, carried low copy numbers of the transgene, and two lines, rabbits 7 and 8, carried high copy numbers (Fig. 2B). The founder of line 16 carried both high T2

**TABLE 1.** Number of Animals and Zygotes used to Generate Tg Rabbits

| | |
|---|---|
| Donor rabbits (total) | 36 |
| Zygotes recovered (total) | 800 |
| Fertilized zygotes (%) | 540 (68) |
| Zygotes microinjected (%) | 456 (84) |
| Zygotes implanted (%) | 456 |
| Zygotes implanted per recipient rabbit (mean ± SD) | 27 ± 3 |
| Recipient rabbits | 17 |
| Pregnancy rate (%) | 12 (71) |
| Gestation period (days, mean ± SD) | 32 ± 1 |
| Rabbits born (total) | 80 |
| Transgenic positive (F0) rabbit (surviving) | 12 (10) |
| Founders that passed the transgene onto their offspring | 6 |

TABLE 2. Characteristics of Six Lines of Tg Rabbits

| Line | Site of Insertion | Estimated Copy Number | Ratio of Transgene to Endogenous Opsin mRNA | Amplitude of Maximum Scotopic ERG a-Wave at 12 Wk (μV) |
|---|---|---|---|---|
| 7 | 13q | 30 | 4:1 | 49.6 ± 12.7 ($n$ = 5) |
| 8 | 12q | 10 | 1:1 | 96.5 ± 20.1 ($n$ = 5) |
| 10 | 2q | 1 | 0.15:1 | 180.2 ($n$ = 1) |
| 11 | Xq | 3 | 0.07:1 | 165.1 ($n$ = 1) |
| 14 | 9p | 3 | 0.1:1 | 159.3 ($n$ = 1) |
| 16* | 6q, 3p | Variable | Variable | Variable |

Maximum scotopic ERGs (mixed rod and cone response) were measured with high intensity flash stimulus of 2.2 log cd · s · $m^{-2}$. Results are expressed as the mean ± SD. The a-wave amplitude of WT NZW rabbits was 170 ± 28 μV ($n$ = 5).

* Double copy line.

and low copy numbers with transgene insertions on different chromosomes that yielded two different lines, 16a and 16b (Fig. 2B).

The transgene copy number estimated by Southern blot analysis correlated roughly with the level of transgene expression and the degree of photoreceptor degeneration as determined by the ERG a-wave amplitude (Table 2). Lines 7 and 8, which had higher transgene copy numbers, had higher levels of transgene expression and showed a rapid, progressive reduction in the a-wave amplitude. In contrast, lines 10, 11, and 14, which had lower copy numbers, had lower transgene expression levels, and the a-wave amplitude was not significantly different from that of age-matched (12 weeks of age) WT rabbits. The a-wave amplitudes for these three lines remained within the normal range, even at 48 weeks (data not shown).

Because of a restriction in the number of rabbits that could be housed in our animal facilities, we mainly produced and investigated line 7, which had the highest level of transgene expression and the most severe photoreceptor degeneration.

## Clinical Findings

Tg rabbits from all lines had normal corneas, anterior chambers, and clear lenses. There was no difference in the fundus appearance or fluorescein angiograms between WT and Tg rabbits at any age up to 40 weeks (Fig. 3). However, it should be noted that Tg animals were on an albino background, and the characteristic bone spicule pigmentation of the retina seen in RP eyes would therefore not be expected.

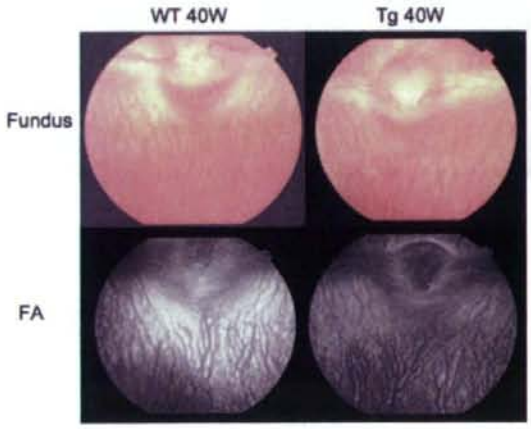


FIGURE 3. Fundus photographs (*top*) and fluorescein angiograms (*bottom*) obtained from a 40-week-old WT and a rhodopsin P347L Tg rabbit from line 7. The appearances of the fundus and the angiogram of the Tg rabbit were indistinguishable from those of the WT rabbit, even at 40 weeks.

## Retinal Histology and Immunohistochemistry

Retinal histology in the area of the visual streak, the central area of the rabbit retina, of a WT and a line 7 Tg rabbit at different ages are shown in Figure 4A. At 2 weeks of age, the retinal histology of Tg rabbits was nearly indistinguishable from that of WT rabbits. Both types of rabbits had six or seven layers of nuclei in the ONL. Thereafter, the thickness of the ONL in Tg rabbits progressively decreased (Fig. 4B). At 48 weeks, only a single row of nuclei remained in the ONL of the retina of Tg rabbits. In contrast, the architecture and thickness of the middle and inner retinal layers were relatively well preserved even at 48 weeks of age.

We also examined the retina of Tg rabbits by immunohistochemistry using an anti-rhodopsin antibody and PNA lectin. There was no detectable rhodopsin labeling in the retina of 48-week-old Tg rabbit in the area of the visual streak (Fig. 5). The cone inner and outer segments were stained by PNA, but their structures were severely disrupted in the 48-week-old Tg rabbit.

There were distinct regional differences in the degree of photoreceptor loss in the older Tg rabbits. The retinal sections from 12-week-old WT and Tg rabbits at three locations along the vertical meridian are shown in Figure 4C. It is known that in normal rabbits, the density of rod and cone photoreceptors is highest at the visual streak located inferior to the optic nerve head.[20] Consistent with previous reports, the thickness of the ONL in WT rabbits was at its maximum near the visual streak. In contrast, the ONL in Tg rabbits was thinnest near the visual streak and was relatively preserved in the peripheral retina (Fig. 4D).

## ERGs of Tg Rabbits

To evaluate the retinal function of the rod and cone systems of Tg rabbits, we recorded full-field scotopic and photopic ERGs. The scotopic and photopic ERGs elicited by different stimulus intensities from a 12-week-old WT and 12- and 48-week-old Tg rabbits are shown in Figures 6A and 6B, respectively. Compared with the ERGs recorded from 12-week-old WT rabbits, the ERG amplitudes of Tg rabbits were clearly reduced at 12 weeks, and the degree of reduction became more severe at 48 weeks. The amplitude of the maximum rod a-wave, which reflects rod photoreceptor activity, was 28% of the WT at 12 weeks and reduced to 5% at 48 weeks (Fig. 6C). In contrast, the maximum cone a-wave amplitude was 65% of the WT at 12 weeks and remained at 35% even at 48 weeks (Fig. 6D). The a-wave fitting model of Hood and Birch[28] also revealed that not only the maximum response amplitude ($Rm$), but also the

COLOR

tapraid4/z7g-iovs/z7g-iovs/z7g00309/z7g9560d09a | moyerr | S=12 | 12/30/08 | 16:42 | Art: 08-2863 | Input-mr



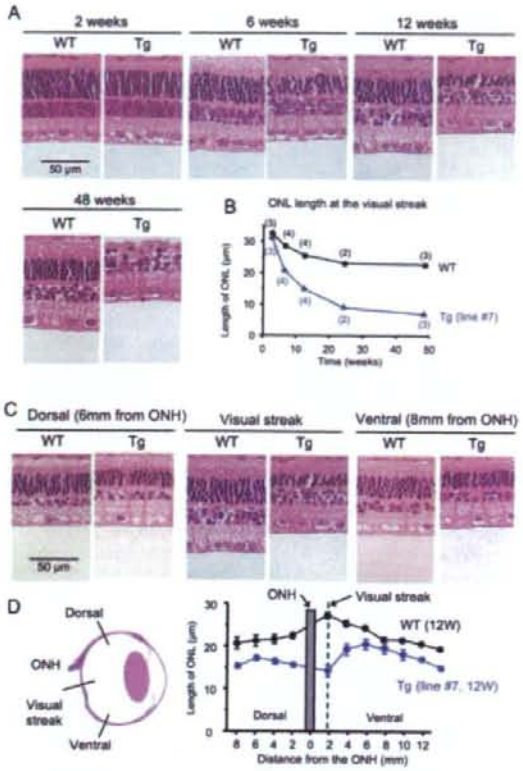


FIGURE 4. Retinal histology of Tg rabbits (line 7). (**A**) Retinal sections of WT and Tg rabbits at 2, 6, 12, and 48 weeks of age. (**B**) Changes in the thickness of the ONL at different ages (in weeks) for WT and Tg rabbits. The number of animals examined is shown in parentheses. (**C**) Vertical retinal sections 6 mm superior to the optic nerve head (ONH), at the visual streak, and 8 mm inferior to the ONH of 12-week-old WT and Tg rabbits. (**D**) Thickness of the ONL along the vertical meridian measured at 10 retinal locations at 2-mm intervals. Mean ± SEM of five WT and five Tg rabbits are plotted.

transduction sensitivity (*S*) were abnormal in both rod and cone photoreceptors of Tg rabbits (Table 3). These results indicated a rod-dominant, progressive photoreceptor dysfunction in the retina of this line of Tg rabbits.

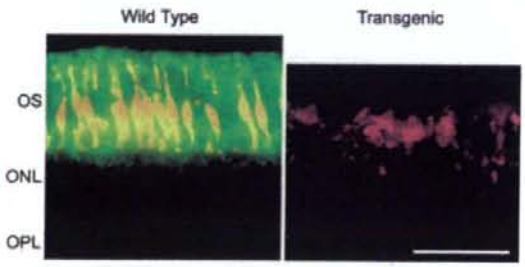


FIGURE 5. Immunohistochemical analysis of rod and cone photoreceptors double labeled with rhodopsin (*green*) and PNA (*red*) at the visual streak of 48-week-old WT (*left*) and transgenic (*right*) rabbits. Bar, 50 μm.

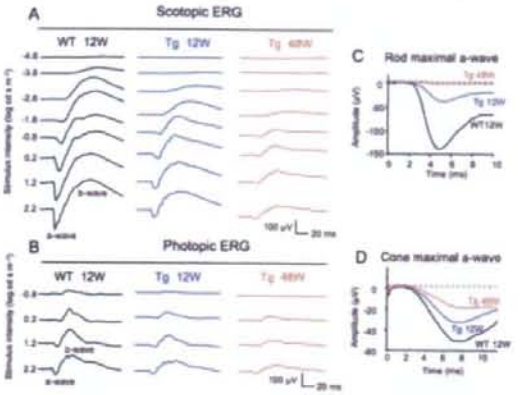


FIGURE 6. ERGs recorded from 12-week-old WT and 12- and 48-week-old rhodopsin P347L (line 7) Tg rabbits. (**A**) Scotopic ERGs elicited by eight different stimulus intensities. (**B**) Photopic ERGs elicited by four different stimulus intensities. (**C**) Rod maximum a-waves elicited by 2.2 log cd · s · $m^{-2}$. These responses were obtained by waveform subtraction of photopic ERGs from scotopic ERGs. (**D**) Cone maximum a-waves elicited by 2.2 log cd · s · $m^{-2}$ on a rod-suppressing white background of 1.3 log cd · s · $m^{-2}$.

## Presence of Extracellular Vesicles in the Tg Rabbit Retina

Finally, we compared the retinal ultrastructure of 6-week-old WT and line 7 Tg rabbits. The outer segments of the photoreceptors were slightly shorter and less organized in the retinas of 6-week-old Tg rabbits, although the outer segments still contained many well-packed discs at this age (Fig. 7A). F7

A striking finding in the Tg rabbit retina was the large number of small vesicles that accumulated in the extracellular space of the photoreceptors (Fig. 7A, asterisks). The vesicles were 50 to 300 nm in size and bound to a single membrane. We also found that these vesicles were cleaved from the membranes of the inner segments of the photoreceptors (Fig. 7B, arrows).

## Discussion

The purpose of this study was to generate a rabbit model of progressive retinal degeneration and to characterize the pattern of degeneration by using histology and electrophysiology. For this purpose, we used rabbit BAC transgenesis, which permitted us to produce a point mutation with no effect on the rest of the large rhodopsin gene, including the regulatory regions of the rhodopsin gene.[22–24] BAC transgenesis is known to provide high tissue- and stage-specific transgene expression that is independent of the site of integration and dependent on the number of integrated copies.[25]

We succeeded in generating six lines of Tg rabbits with different expression levels. Two lines showed high transgene expression levels and progressive retinal degeneration. Retinal histologic and ERG studies showed early loss of rod function associated with relatively preserved cone function, which is very similar to the clinical findings of human RP patients with the rhodopsin P347L mutation.[30,31] To the best of our knowledge, this is the first rabbit model of progressive retinal degeneration. Because rabbits have large eyes and are easy to handle and breed, we believe that our Tg rabbits are useful animal models for testing various new treatments, including surgical procedures.

tapraid4/z7g-iovs/z7g-iovs/z7g00309/z7g9560d09a | moyerr | S=12 | 12/30/08 | 16:42 | Art: 08-2863 | Input-mr



TABLE 3. Summary of Photoreceptor Function Parameters in Transgenic Rabbits

| | 12 Wk | | 48 Wk | |
|---|---|---|---|---|
| | WT | Tg | WT | Tg |
| Rod log *Rm* (maximum response) | 2.23 ± 0.08 | 1.63 ± 0.06* | 2.06 ± 0.10 | —† |
| Rod log *S* (sensitivity) | 3.50 ± 0.04 | 3.19 ± 0.11* | 3.42 ± 0.06 | —† |
| Cone log *Rm* (maximum response) | 1.73 ± 0.09 | 1.47 ± 0.07* | 1.64 ± 0.08 | 1.21 ± 0.23* |
| Cone log *S* (sensitivity) | 2.97 ± 0.05 | 2.84 ± 0.14 | 2.93 ± 0.10 | 2.68 ± 0.18* |

Data are expressed as the mean ±SD. $n = 5$ for all.

* $P < 0.05$ (unpaired *t*-test).

† Rod photoreceptor responses in 48-week-old Tg rabbits were too small for the fitting model to be applied.

The fundus appearance and fluorescein angiograms were nearly normal in our Tg rabbits. The blood vessel diameters and optic disc appearance were examined monthly, and they were indistinguishable between WT and Tg rabbits at ages up to 40 weeks. An early sign of RP in human patients is an attenuation of blood vessel diameters in the eye. The normal diameter of the retinal vessels in our Tg rabbits may be due to the characteristics of rabbit retina, because retinal vessels in rabbits are confined to the horizontal myelinated bands, comprising optic axons, oligodendrocytes, and astrocytes, and are not associated with the inner retinal layers, as in vascular retinas.

In this study, we generated the transgenic rabbits on an albino background (NZW), because the rabbit BAC library was available only for NZW rabbits. However, this albino background may limit the model's usefulness. First, normal fundus coloring without any pigmentation in our Tg rabbits may have occurred because we used the nonpigmented NZW rabbits. Second, it is known that there are other anomalies in the visual system of albino rabbits, including lower ganglion cell densities[32] and aberrant optic decussation and retinal projections. To overcome these limitations, we are currently producing a pigmented line of Tg rabbits by mating our NZW Tg rabbits with pigmented Dutch rabbits.

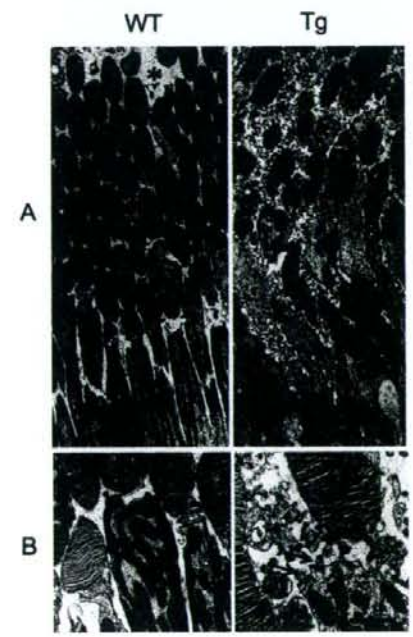


FIGURE 7. Ultrastructural analyses of 6-week-old WT (*left*) and Tg (*right*) rabbit retinas. (**A**) Tg rabbit retina showing many small vesicles accumulated in the extracellular space (✱). (**B**) These abnormal vesicles were cleaved from the inner segment of photoreceptors (*arrows*).

By measuring the ONL thickness at different locations along the vertical meridian, we found a marked regional variation in the loss of photoreceptors in the Tg rabbit retina. The loss of photoreceptors was at its maximum near the visual streak, where the photoreceptor density is highest in WT rabbits. In contrast, the ONL thickness in Tg rabbits was relatively preserved in the peripheral retina (Figs. 4C, 4D). Similar regional variations in photoreceptor loss have been reported in other large animal models, including pigs and dogs.[16,17] Such regional variation in photoreceptor loss may be due to topographic variations in opsin expression, as reported by Timmers et al.,[33] and van Ginkel et al.,[34] who showed a central-to-peripheral gradient of rhodopsin mRNA levels in bovine retinas.

A distinct ultrastructural observation in the retina of Tg rabbits was the accumulation of numerous extracellular vesicles that were cleaved from the inner segments of the photoreceptors. At this stage, the outer segments still contained well-packed discs. These findings are consistent with findings in Tg mice with the P347S rhodopsin mutation.[35] Using two monoclonal antibodies against rhodopsin, Li et al.[35] demonstrated that these small vesicles contain rhodopsin, and they proposed that they were produced as a consequence of a defect in the transport of rhodopsin from the inner segment to the disc membranes of the outer segments. Although we have not yet examined whether the vesicles contain rhodopsin in our Tg rabbits, the similarity in the ultrastructural findings and site of rhodopsin mutation suggested that the defective delivery of opsin to the outer segment may be one of the causes of photoreceptor cell death in our Tg rabbits. However, other factors, including an overexpression of rhodopsin,[36,37] prolonged activation of phototransduction,[38] or activation of mislocalized opsin,[39] may be involved.

In conclusion, we have succeeded in generating a Tg rabbit model of retinal degeneration. Although further studies are needed to determine the exact mechanism of photoreceptor death observed in our model, we believe that our Tg rabbits will serve as a useful midsized animal model with which to study the pathophysiology of RP and develop novel treatments.

## *Acknowledgments*

The authors thank Kensaku Kitada (Kitayama Labes Co., Nagano, Japan) for breeding the Tg rabbits; Akira Shiota (PhoenixBio Co., Ltd. Tochigi, Japan) for technical help with BAC transgenesis; Robert E. Marc and Bryan W. Jones of Utah University for critical comments on the manuscript; and Prof. Hamasaki of Miami University and Yozo Miyake of Shukutoku University for discussions of the manuscript.

AQ: 4

## *References*

1. Heckenlively JR. RP syndromes. In: Heckenlively JR, ed. *Retinitis Pigmentosa*. Philadelphia: JB Lippincott; 1988:221–252.
2. Weleber RG, Gregory-Evance K. Retinitis pigmentosa and allied disorders. In: Hinton DR, ed. *Basic Science and Inherited Retinal Disease: Retina*. Vol. 1, 4th ed. St. Louis: Mosby; 2006:395–498.
3. Hartong DT, Berson EL, Dryja TP. Retinitis pigmentosa. *Lancet*. 2006;368:1795–1809.
4. Daiger SP, Bowne SJ, Sullivan LS. Perspective on genes and mutations causing retinitis pigmentosa. *Arch Ophthalmol*. 2007;125:151–158.
5. Gal A, Apfelstedt-Sylla E, Janecke AR, Zrenner E. Rhodopsin mutations in inherited retinal dystrophies and dysfunctions. *Prog Retin Eye Res*. 1997;16:51–79.
6. Dryja TP, Hahn LB, Cowley GS, et al. Mutation spectrum of the rhodopsin gene among patients with autosomal dominant retinitis pigmentosa. *Proc Natl Acad Sci USA*. 1991;88:9370–9374.
7. Petersen-Jones SM. Animal models of human retinal dystrophies. *Eye*. 1998;12:566–570.
8. Chader GJ. Animal models in research on retinal degenerations: past progress and future hope. *Vision Res*. 2002;42:393–399.
9. Tao W, Wen R, Goddard MB, et al. Encapsulated cell-based delivery of CNTF reduces photoreceptor degeneration in animal models of retinitis pigmentosa. *Invest Ophthalmol Vis Sci*. 2002;43:3292–3298.
10. Bush RA, Lei B, Tao W, et al. Encapsulated cell-based intraocular delivery of ciliary neurotrophic factor in normal rabbit: dose-dependent effects on ERG and retinal histology. *Invest Ophthalmol Vis Sci*. 2004;45:2420–2430.
11. Acland GM, Aguirre GD, Ray J, et al. Gene therapy restores vision in a canine model of childhood blindness. *Nat Genet*. 2001;28:92–95.
12. Güven D, Weiland JD, Fujii G, et al. Long-term stimulation by active epiretinal implants in normal and RCD1 dogs. *J Neural Eng*. 2005;2:S65–73.
13. Narfström K. Hereditary progressive retinal atrophy in the Abyssinian cat. *J Hered*. 1983;74:273–276.
14. Menotti-Raymond M, David VA, Schäffer AA, et al. Mutation in CEP290 discovered for cat model of human retinal degeneration. *J Hered*. 2007;98:211–220.
15. Acland GM, Fletcher RT, Gentleman S, et al. Non-allelism of three genes (rcd1, rcd2 and erd) for early-onset hereditary retinal degeneration. *Exp Eye Res*. 1989;49:983–998.
16. Kijas JW, Cideciyan AV, Aleman TS, et al. Naturally occurring rhodopsin mutation in the dog causes retinal dysfunction and degeneration mimicking human dominant retinitis pigmentosa. *Proc Natl Acad Sci USA*. 2002;99:6328–6333.
17. Petters RM, Alexander CA, Wells KD, et al. Genetically engineered large animal model for studying cone photoreceptor survival and degeneration in retinitis pigmentosa. *Nat Biotechnol*. 1997;15:965–970.
18. Marc RE. Neurochemical stratification in the inner plexiform layer of the vertebrate retina. *Vision Res*. 1986;26:223–238.
19. Vaney DI, Young HM, Gynther IC. The rod circuit in the rabbit retina. *Vis Neurosci*. 1991;7:141–154.
20. Famiglietti EV, Sharpe SJ. Regional topography of rod and immunocytochemically characterized "blue" and "green" cone photoreceptors in rabbit retina. *Vis Neurosci*. 1995;12:1151–1175.
21. Rockhill RL, Daly FJ, MacNeil MA, et al. The diversity of ganglion cells in a mammalian retina. *J Neurosci*. 2002;22:3831–3843.
22. Yang XW, Model P, Heintz N. Homologous recombination based modification in Escherichia coli and germline transmission in transgenic mice of a bacterial artificial chromosome. *Nat Biotechnol*. 1997;15:859–865.
23. Zhang Y, Buchholz F, Muyrers JP, Stewart AF. A new logic for DNA engineering using recombination in Escherichia coli. *Nat Genet*. 1998;20:123–128.
24. Muyrers JP, Zhang Y, Benes V, et al. Point mutation of bacterial artificial chromosomes by ET recombination. *EMBO Rep*. 2000;1:239–243.
25. Giraldo P, Montoliu L. Size matters: use of YACs, BACs and PACs in transgenic animals. *Transgenic Res*. 2001;10:83–103.
26. Abe K, Hazama M, Katoh H, et al. Establishment of an efficient BAC transgenesis protocol and its application to functional characterization of the mouse Brachyury locus. *Exp Anim*. 2004;53:311–320.
27. Committee for Standardized Karyotype of Oryctolagus Cuniculus. Standard karyotype of the laboratory rabbit, Oryctolagus cuniculus. *Cytogenet Cell Genet*. 1981;31:240–248.
28. Hood DC, Birch DG. Rod phototransduction in retinitis pigmentosa: estimation and interpretation of parameters derived from the rod a-wave. *Invest Ophthalmol Vis Sci*. 1994;35:2948–2961.
29. Blanks JC, Johnson LV. Specific binding of peanut lectin to a class of retinal photoreceptor cells: a species comparison. *Invest Ophthalmol Vis Sci*. 1984;25:546–557.
30. Oh KT, Longmuir R, Oh DM, Stone EM, et al. Comparison of the clinical expression of retinitis pigmentosa associated with rhodopsin mutations at codon 347 and codon 23. *Am J Ophthalmol*. 2003;136:306–313.
31. Berson EL, Rosner B, Sandberg MA, et al. Ocular findings in patients with autosomal dominant retinitis pigmentosa and rhodopsin, proline-347-leucine. *Am J Ophthalmol*. 1991;111:614–623.
32. Oyster CW, Takahashi ES, Fry KR, Lam DM. Ganglion cell density in albino and pigmented rabbit retinas labeled with a ganglion cell-specific monoclonal antibody. *Brain Res*. 1987:425;25–33.
33. Timmers AM, Wintjes ET, Hauswirth WW. Fetal topography of bovine rhodopsin mRNA suggests retinotopographically determined gene expression. *Invest Ophthalmol Vis Sci*. 1995;36:2008–2019.
34. van Ginkel PR, Timmers AM, Szél A, Hauswirth WW. Topographical regulation of cone and rod opsin genes: parallel, position dependent levels of transcription. *Brain Res Dev Brain Res*. 1995;89:146–149.
35. Li T, Snyder WK, Olsson JE, Dryja TP. Transgenic mice carrying the dominant rhodopsin mutation P347S: evidence for defective vectorial transport of rhodopsin to the outer segments. *Proc Natl Acad Sci USA*. 1996;93:14176–14181.
36. Olsson JE, Gordon JW, Pawlyk BS, et al. Transgenic mice with a rhodopsin mutation (Pro23His): a mouse model of autosomal dominant retinitis pigmentosa. *Neuron*. 1992;9:815–830.
37. Tan E, Wang Q, Quiambao AB, et al. The relationship between opsin overexpression and photoreceptor degeneration. *Invest Ophthalmol Vis Sci*. 2001;42:589–600.
38. Chen J, Makino CL, Peachey NS, Baylor DA, Simon MI. Mechanisms of rhodopsin inactivation in vivo as revealed by a COOH-terminal truncation mutant. *Science*. 1995;267:374–377.
39. Alfinito PD, Townes-Anderson E. Activation of mislocalized opsin kills rod cells: a novel mechanism for rod cell death in retinal disease. *Proc Natl Acad Sci USA*. 2002;99:5655–5660.

*Clinical and Experimental Ophthalmology* 2008; **36**: 782–785
doi: 10.1111/j.1442-9071.2008.01887.x

# Clinicopathological Report

## Removal of internal limiting membrane for recurrent myopic traction maculopathy

**Sou Futagami MD, Makoto Inoue MD and Akito Hirakata MD**
Kyorin Eye Center, Kyorin University School of Medicine, Tokyo, Japan

### Abstract

A 63-year-old man presented with a foveal detachment and retinoschisis associated with myopic traction maculopathy of his left eye with a refractive error of −12.0 dioptres. Both the retinoschisis and foveal detachment were initially successfully treated with vitreous surgery that was limited to the induction of a posterior vitreous detachment beyond the areas of retinoschisis over the posterior staphyloma. Three years later, the macula re-detached and further surgery was performed, which involved peeling the internal limiting membrane (ILM). Following the second vitreous surgery the macula reattached within one month of the surgery and this success has been sustained for 2 years, suggesting that peeling the ILM may be an effective treatment for recurrent myopic traction maculopathy.

**Key words:** high myopia, internal limiting membrane, myopic traction maculopathy, retinoschisis, vitrectomy.

### Introduction

Myopic traction maculopathy with foveal detachment and retinoschisis has been described as one of the complications of highly myopic eyes with a posterior staphyloma.[1,2] Optical coherence tomographic (OCT) studies have detected foveal detachments and retinoschisis in many severely myopic eyes with a posterior staphyloma.[1,2] Vitrectomy with vitreous cortex removal, internal limiting membrane (ILM) peeling and gas tamponade has been found to be effective in treating myopic traction maculopathy.[3–5] However, the efficacy of ILM peeling is still controversial because myopic traction maculopathy could be reattached by removal of the posterior hyaloid membrane without ILM peeling.[6,7] We present a case of myopic traction maculopathy that was treated with vitrectomy to create a posterior vitreous detachment (PVD) to treat the maculopathy. However, 3 years later the maculopathy recurred, and vitrectomy with ILM peeling was performed that led to a retinal reattachment.

### Case report

A 63-year-old man presented on March 2002 with a 6-month history of metamorphopsia in his left eye. His best-corrected visual acuity (BCVA) was 6/7.5 right eye (OD) and 6/15 left eye (OS) with refractive errors of −13.0 dioptres (D) OD and −12.0 D OS. Both eyes had moderate cataracts, and the intraocular pressure was 16 mmHg OD and 15 mmHg OS. Ophthalmoscopy showed a serous macular detachment over the posterior staphyloma in the left eye (Fig. 1a). OCT (OCT2; Carl Zeiss Meditec, Dublin, CA, USA) revealed intraretinal dehiscence around the macula and a slight elevation of the fovea (Fig. 1b). The patient was diagnosed as having a foveal detachment and retinoschisis associated with myopic traction maculopathy in the left eye. Vitreous surgery was performed in April 2002 after a written informed consent was obtained. Intraoperatively, the vitreous was liquefied, and vitreous gel was not detected in the centre of the vitreous body, but the gel appeared to have accumulated in the periphery of the vitreous. After core vitrectomy, the posterior vitreous cortex was separated from the posterior retinal surface with a bent microvitreoretinal knife (20-G) to create a flap of the posterior vitreous cortex. Then, viscodissection was performed by injecting a viscoelastic agent (Healon, AMO, CA, USA) through the window of the posterior vitreous cortex to separate the posterior hyaloid over the retinoschisis in the posterior staphyloma. A PVD was created over the posterior staphyloma through the equator, but gas was not injected into the vitreous cavity. Triamcinolone acetonide was not used intraoperatively to highlight the posterior hyaloid membrane. Cataract extraction was performed as a result of a nuclear cataract 8 months later. The foveal detachment and retinoschisis gradually decreased and the retina was completely reattached 1 year after surgery

■ *Correspondence*: Associate Professor Makoto Inoue, Kyorin Eye Center, Kyorin University School of Medicine, 6-20-2 Shinkawa, Mitaka, Tokyo 181-8611, Japan. Email: inoue@eye-center.org

*Received 15 July 2008, accepted 1 October 2008.*

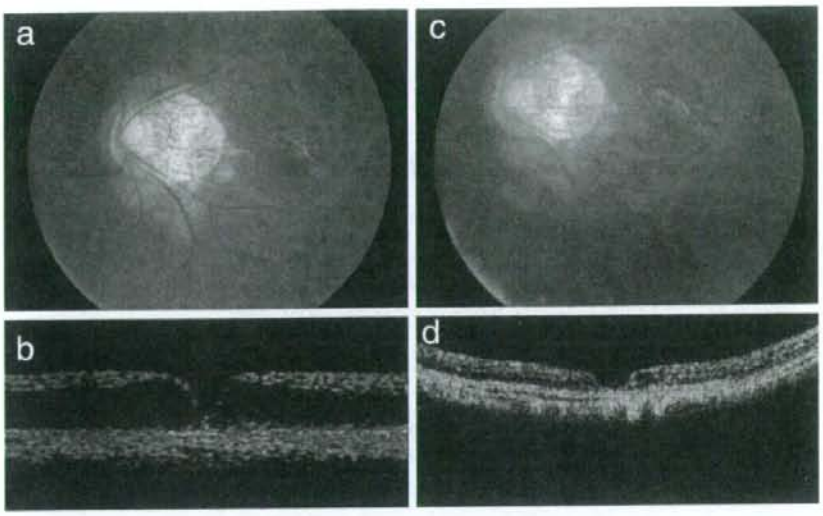


**Figure 1.** Fundus photographs and optical coherence tomographic (OCT) images before and after the initial surgery. (a) Preoperative fundus photograph at presentation showing a shallow macular detachment over the posterior staphyloma. (b) Preoperative OCT image (OCT2) showing posterior retinoschisis and shallow foveal detachment. (c) Photograph one year after surgery showing macular reattachment. (d) Postoperative OCT image (OCT3) showing an absence of retinoschisis and foveal detachment.

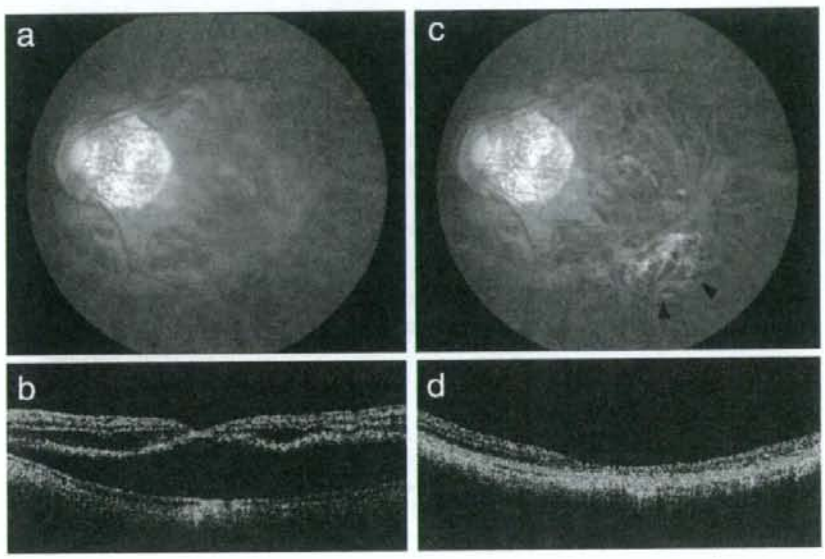


**Figure 2.** Fundus photographs and optical coherence tomographic (OCT) images before and after the second surgery. (a) Photograph showing a recurrent macular detachment over the posterior staphyloma 3 years after the initial surgery. (b) Preoperative OCT image (OCT3) showing recurrent posterior retinoschisis and foveal detachment. (c,d) Postoperative photograph (c) and OCT image (d) 3 months after surgery showing a complete resolution of the retinoschisis and foveal detachment. Arrowheads indicate the enlarged atrophy around the photocoagulation for the iatrogenic retinal break.

(Fig. 1c,d). The vision remained at 6/15 but with improvement of the symptoms.

Three years later, the vision in the left eye decreased to 6/60. Ophthalmoscopy and OCT (OCT3; Carl Zeiss Meditec, Dublin, California, USA) showed a macular detachment and retinoschisis, indicating a recurrence of the myopic traction maculopathy (Fig. 2a,b). A second vitrectomy with extensive ILM peeling was performed on May 2005. A small iatrogenic retinal break was created during ILM peeling, and subretinal fluid was not drained through the break. Photocoagulation was applied around the retinal break under intravitreal perfluorocarbon tamponade. Subsequently, 20% $SF_6$ gas was injected into the vitreous cavity. A complete retinal reattachment was achieved after one month, and vision recovered to 6/30 without any recurrence of myopic traction maculopathy up to the last visit 2 years after the surgery (Fig. 2c,d).

Electron microscopic examination of the excised membrane revealed that most of the tissue consisted of only the ILM with smooth surfaces. There were multiple layers of proliferated cells on some areas of the ILM (Fig. 3a). Higher magnification of the cells showed multiple highly dense, intracytoplasmic granules, cytoplasmic processes and basal lamina, suggestive of retinal pigment epithelial cells (Fig. 3b). There were thin collagen fibres between proliferative cells and the ILM.

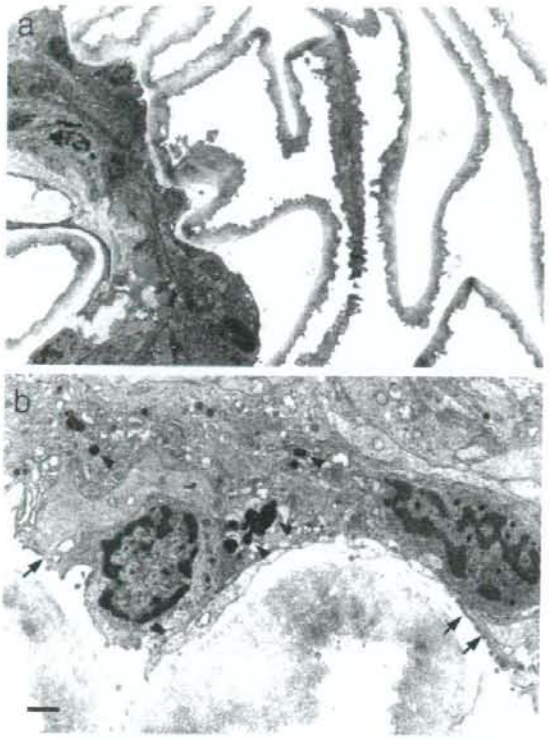


**Figure 3.** Electron microscopic analyses of the excised internal limiting membrane (ILM). (a) Low magnification electron photomicrograph of the excised ILM showing multiple layers of proliferated cells on the smooth surface of the ILM. (b) Higher magnification electron photomicrograph of the excised ILM showing many high density intracytoplasmic granules (arrowheads), cytoplasmic processes and basal lamina (arrows), suggestive of retinal pigment epithelial cells (bar, 1 μm).

## Discussion

The appearance of a posterior vitreous adhesions over the macula in eyes with myopic traction maculopathy is similar to that seen in eyes with a retinal detachment associated with a macular hole.[3] Because the release of vitreous traction by vitrectomy and creation of a PVD can lead to closure of macular holes, similar surgery should also be successful in treating myopic traction maculopathy. This was confirmed by Spaide *et al.*,[6] who reported that vitrectomy without ILM peeling followed by gas tamponade resulted in successful visual and anatomical outcomes on eyes with myopic traction maculopathy. We have also found that creating a PVD without ILM peeling could reattach the retinoschisis in some eyes with a myopic traction maculopathy.[7]

On the other hands, traction by the ILM may be responsible for myopic traction maculopathy in other eyes.[3–5] Clinicopathological report of excised ILMs from patients with myopic traction maculopathy showed that collagen fibre and fibrous glial cells were present on the inner surface of the ILM.[8] The authors concluded that collagen fibres and cellular components played a role in the development of myopic traction maculopathy. Our case had a complete resolution of the myopic traction maculopathy after the removal of the posterior hyaloid vitreous traction at the initial surgery. However, a recurrent myopic traction maculopathy developed 3 years after surgery.

Electron microscopic examinations showed cellular proliferation on the ILM. Because the removal of the ILM resulted in resolution of the myopic traction maculopathy, this suggests that the proliferative cells may have caused the tangential traction of the ILM to induce the retinal detachment and retinoschisis. We assume that chronic vitreous traction in eyes with myopic traction maculopathy may induce cellular migration of retinal pigment epithelial cells onto the retina even without macular hole. Earlier studies have shown that ILM peeling is effective in preventing a reopening of an idiopathic macular hole.[10] Thus, ILM peeling may not only lead to a resolution of the retinoschisis but also be effective in preventing a recurrence of the myopic traction maculopathy.

In summary, vitrectomy with ILM removal can be effective in reattaching a detached retina and retinoschisis in eyes with recurrent myopic traction maculopathy. However, further studies are needed to evaluate the complications of ILM removal, and the use of more recent surgical techniques including observation of the vitreous cortex by intravitreal triamcinolone acetonide to induce a more complete PVD.

## Acknowledgements

No author has a financial or proprietary interest in any material or method mentioned. Author contributions: Design of the study (SF, AH); Conduct of the study (AH); Collection and Analysis of the data (AH, MI); Literature Search (AH, MI).

## References

1. Takano M, Kishi S. Foveal retinoschisis and retinal detachment in severely myopic eyes with posterior staphyloma. *Am J Ophthalmol* 1999; **128**: 472–6.
2. Panozzo G, Mercanti A. Optical coherence tomography findings in myopic traction maculopathy. *Arch Ophthalmol* 2004; **122**: 1455–60.
3. Panozzo G, Mercanti A. Vitrectomy for myopic traction maculopathy. *Arch Ophthalmol* 2007; **125**: 767–72.
4. Ikuno Y, Sayanagi K, Ohji M *et al.* Vitrectomy and internal limiting membrane peeling for myopic foveoschisis. *Am J Ophthalmol* 2004; **137**: 719–24.
5. Kanda S, Uemura A, Sakamoto Y, Kita H. Vitrectomy with internal limiting membrane peeling for macular retinoschisis and retinal detachment without macular hole in highly myopic eyes. *Am J Ophthalmol* 2003; **136**: 177–80.
6. Spaide RF, Fisher Y. Removal of adherent cortical vitreous plaques without removing the internal limiting membrane in

the repair of macular detachments in highly myopic eyes. *Retina* 2005; **25**: 290–95.
7. Hirakata A, Hida T. Vitrectomy for myopic posterior retinoschisis or foveal detachment. *Jpn J Ophthalmol* 2006; **50**: 53–61.
8. Oshima Y, Ikuno Y, Motokura M *et al.* Complete epiretinal membrane separation in highly myopic eyes with retinal detachment resulting from a macular hole. *Am J Ophthalmol* 1998; **126**: 669–76.
9. Bando H, Ikuno Y, Choi JS *et al.* Ultrastructure of internal limiting membrane in myopic foveoschisis. *Am J Ophthalmol* 2005; **139**: 197–9.
10. Brooks HL Jr. Macular hole surgery with and without internal limiting membrane peeling. *Ophthalmology* 2000; **107**: 1939–48.

# Correlation between Macular Volume and Focal Macular Electroretinogram in Patients with Retinitis Pigmentosa

*Tadasu Sugita, Mineo Kondo, Chang-Hua Piao, Yasuki Ito, and Hiroko Terasaki*

**Purpose.** To determine whether a significant correlation exists between the morphology of the macula measured by optical coherence tomography (OCT) and the amplitude of focal macular electroretinograms (fmERGs) in patients with retinitis pigmentosa (RP).

**Methods.** fmERGs were recorded in 43 patients with RP and 43 age-similar normal subjects, with a 15° stimulus spot, 5.6 to 5.8 mm in diameter on the fundus. The sum of the volume of the neural retina in the central 6 mm (total macular volume) was measured with the OCT system. The length of the photoreceptor inner segment/outer segment junction (IS/OS line) in a 6-mm diameter macular area was also measured in the OCT images.

**Results.** There was a weak correlation between the total macular volume and the fmERG amplitudes (correlation coefficient, 0.46 for the a-wave and 0.54 for the b-wave). The fmERG amplitudes in the patients with RP with IS/OS line longer than 2 mm were significantly larger than those in patients with RP with IS/OS line shorter than 2 mm, but the correlations between these two factors were weak. One major reason for the low correlations between the macular morphology and fmERGs was that there were some patients with RP who had normal macular volume and long IS/OS line, but had severely reduced focal macular ERGs.

**Conclusions.** Although the macular volume and length of the IS/OS line correlated weakly with the amplitude of the fmERGs, a preserved macular morphology does not necessarily guarantee normal-amplitude fmERGs in patients with RP. (*Invest Ophthalmol Vis Sci.* 2008;49:3551–3558) DOI:10.1167/iovs.08-1954

Retinitis pigmentosa (RP) is a subset of inherited retinal diseases characterized by a progressive loss of the rod and cone photoreceptors.[1–5] Past histopathologic studies on patients with RP[6–8] have shown that the earliest anatomic change is a shortening or distortion of the rod and cone photoreceptor outer segments. This change is followed by the loss of rod and cone photoreceptors beginning in the periphery and progressing toward the central retina.

It is important to evaluate the functional and structural changes in the macular area of patients with RP because the central retina is relatively better preserved until the late stages, and various subjective and objective examinations have been used. Focal ERGs[9–13] and multifocal ERGs[14–21] have been used to assess the macular function of eyes with RP, because these techniques can examine the neural activities of the macular area objectively.

Optical coherence tomography (OCT) is a noninvasive technique that can assess the morphology of the retina, especially the macula in vivo. This technique is especially useful in patients with RP, because OCT enables the investigator to evaluate the morphologic changes in each retinal layer and the overall retina.[22–26] It has been shown that the OCT-determined cross-sectional retinal images were well-correlated with retinal histology in animal models of retinal degeneration.[37–40] In addition, there is evidence that the OCT-determined structural changes in the central retina correlate with subjective visual functions including the visual acuity and visual threshold in patients with RP.[27,30,34,36] However, there is only one report on the relationship between the morphologic changes measured by OCT and macular function measured by focal macular ERGs (fmERGs) in patients with RP.[25] The relationship between the macular morphology and function in patients with RP can provide important information on the treatment of patients with retinal degeneration.[29,31–33]

Thus, the purpose of this study was to determine whether a significant correlation exists between the amplitude of the fmERGs and the sum of the volume of the neural retina in the central 6 mm of the macula (total macular volume) or the length of the photoreceptor inner/outer segment junction (IS/OS line) measured by OCT images in patients with typical retinitis pigmentosa (RP).

## Methods

### Subjects

This prospective study included 124 consecutive patients with RP who visited one ophthalmologist (MK) in the Department of Ophthalmology, Nagoya University Hospital, from January to December in 2006. The clinical diagnosis of RP was based on the ocular history, funduscopic findings, visual fields, and ISCEV (International Society for Clinical Electrophysiology of Vision) standard full-field ERGs.[41] The inclusion criteria were a diagnosis of RP with a complete medical examination, including best corrected visual acuity (BCVA) measured by the standard Japanese decimal visual acuity chart, fundus examination, Goldmann kinetic visual fields, full-field ERGs; BCVA had to be ≥0.3. The exclusion criteria were atypical RP (e.g., central RP, sector RP, or unilateral RP), opacities in the media including cataracts, and cystoid macular edema identified by the OCT. Based on these inclusion and exclusion criteria, 43 eyes of 43 patients with RP (19 males, 24 females; mean age, 41.7 years; range, 16–66) were analyzed. If both eyes met these criteria, then the data from only the right eye were used for the analyses.

The inheritance pattern was autosomal dominant in 6 (14%) patients, autosomal recessive in 6 (14%), and sporadic in 31 (72%). None of the patients was found to have X-linked RP. The best corrected visual acuity ranged from 0.3 to 1.2, and the mean logarithm of the minimum angle of resolution (logMAR) was 0.052 units.

For controls, fmERGs and OCT were recorded from 43 age-similar normal subjects (14 males, 29 females; mean age, 42.7 years, range,

From the Department of Ophthalmology, Nagoya University Graduate School of Medicine, Nagoya, Japan.

Supported by Grants-in Aid 18591913 (MK), 19500416 (YI), and 18390466 (HT) from the Ministry of Education, Culture, Sports, Science and Technology.

Submitted for publication February 29, 2008; revised April 13, 2008; accepted June 16, 2008.

Disclosure: **T. Sugita**, None; **M. Kondo**, None; **C.-H. Piao**, None, **Y. Ito**, None; **H. Terasaki**, None

The publication costs of this article were defrayed in part by page charge payment. This article must therefore be marked "*advertisement*" in accordance with 18 U.S.C. §1734 solely to indicate this fact.

Corresponding author: Mineo Kondo, Department of Ophthalmology, Nagoya University Graduate School of Medicine, 65 Tsuruma-cho, Showa-ku, Nagoya 466-8550, Japan; kondomi@med.nagoya-u.ac.jp.

16–67). None had known abnormalities of the visual system, and their visual acuity was ≥1.0 in all.

The research was conducted in accordance with the Institutional Guidelines of Nagoya University and conformed to the tenets of the World Medical Association's Declaration of Helsinki. Informed consent was obtained from each of the patients after they were provided sufficient information on the procedures to be used.

### Focal Macular ERGs

The stimulus and recording systems used to record fmERGs have been described in detail.[13,42,43] Briefly, an infrared fundus camera equipped with a stimulus light, background illumination, and fixation target was used. The image from the camera was fed to a television monitor, and the examiner used the image on the monitor to maintain the stimulus on the macula. A stimulus spot size of 15° was selected because ocular biometry[44–46] has shown that a 15° stimulus spot covers a retinal area of 5.5 to 5.8 mm, which is approximately the size of the OCT-determined macular diameter (6.0 mm). The background light subtended a visual angle of 45°, and additional background illumination outside the central 45° produced a homogeneous background for nearly the entire visual field. The luminances of the white stimulus light and background light were 29.46 and 2.89 cd/m$^2$, respectively. Although this luminance of background light was not strong enough to suppress all the rod activity, we have shown that the fmERGs elicited by this method are generated mainly by the cone system, and the responses elicited by spot stimuli of 5 to 15° are local responses.[42,43]

A Burian-Allen bipolar contact lens electrode was used to record the fmERGs. This contact lens electrode system had low electrical noise and permitted a clear view of the fundus by the camera during the recordings. After the pupils were fully dilated with 0.5% tropicamide and 0.5% phenylephrine hydrochloride, fmERGs were elicited by a flicker train consisting of a square waves presented at 5 Hz (100-ms on and 100-ms off). Then, a series of 512 responses were averaged in a single cycle by a signal processor. The time constant of the bioamplifier was set at 0.03 seconds with a 100-Hz high-cut filter to record the a- and b-waves.

The amplitude of the a-wave was measured from the baseline to the first negative trough, and the amplitude of b-wave was measured from the trough of the a-wave to the positive peak of the b-wave.

### OCT Measurements

The morphology of the macula was evaluated by a high-resolution optical coherence tomograph (Stratus model 3000, software ver. 4.0.1; Carl Zeiss Meditec, AG, Oberkochen, Germany). After the patients' pupils were fully dilated with 0.5% tropicamide and 0.5% phenylephrine, the sum of the volume of the neural retina in the central 6 mm of the macula (total macular volume) was measured using six scans of 6 mm in a radial pattern intersecting at the fixation point.

It is known that the automatic fast macular thickness map (FMTM) protocol often fails to identify the outer borders of the neural retina, which can lead to recording of erroneous retinal thicknesses and volumes.[47] Therefore, we used a program developed in our laboratory (Ishikawa K, et al. *IOVS* 2005;46:ARVO E-Abstract 1550),[48] by which the total macular volume was measured more precisely than that calculated by the conventional FMTM system. In this program, the user was able to set 20 cursors above and below a selected area manually. The inner cursors were set on the internal limiting membrane (ILM), and the outer cursors were set on the retinal pigment epithelium (RPE)–choriocapillaris hyperreflective complex borderline. Another set of cursors was set on the fovea of the OCT images. Then, each OCT radial scan was analyzed as a retinal map, and the total macular volume was calculated precisely by our software.

Past studies with the Stratus OCT and ultrahigh-resolution OCT demonstrated that there are two well-defined, parallel, highly reflective lines (HRLs) in the outer retinal layer.[49,50] It has been shown that the inner HRL corresponds to the photoreceptor inner/outer segment junction or the IS/OS line, and the outer HRL corresponds to the retinal pigment epithelium and choriocapillaris complex. To asses the relationship between the morphologic changes in the photoreceptor layer and the amplitude of the fmERGs, we classified the IS/OS line in patients with RP into three types: type 1, distinct IS/OS line longer than the central 2 mm; type 2, distinct IS/OS line only within the central 2 mm; and type 3, absence of IS/OS line within the central 6 mm (Fig. 1). To perform this classification, we reviewed the six tomographic images of each eye on a gray scale with an alignment image protocol, because the IS/OS line is more clearly visible on gray-scale tomographic images.[51] The classification was performed by TS in a masked manner.

### Statistical Analyses

The significance of the differences between the patients with RP and normal control subjects was determined by nonparametric Mann-Whitney U tests. The correlations between the macular volume and the fmERG amplitudes were determined by the Spearman's rank correlation. Differences in the amplitudes among the three groups (types 1, 2, and 3) based on the length of the IS/OS line were analyzed with the nonparametric Kruskal-Wallis test and Scheffé's test, as the multiple comparison procedures. Differences and correlations were considered to be significant when $P < 0.05$.

## Results

Representative OCT images and fmERGs recorded from one normal subject and three patients with RP are shown in Figure 2. The amplitudes of the fmERGs in case 1 were relatively well preserved, and the macular volume was within the normal range. The amplitudes of the fmERGs in case 2 were reduced, and the macular volume was close to the lower borderline of normal. The fmERGs in case 3 were nonrecordable, and the macular volume was severely reduced.

Box plots of the fmERG amplitudes (a- and b-waves) and total macular volume for 43 normal control subjects and 43 patients with RP are shown in Figure 3. As expected, both the amplitudes of the a- and b-waves of the fmERGs and the total

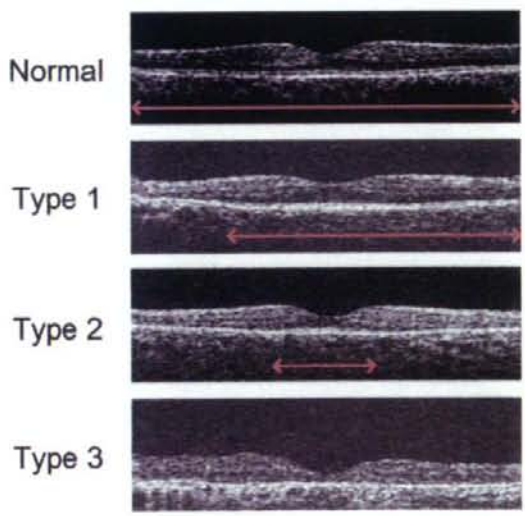


FIGURE 1. The photoreceptor IS/OS junction line in the OCT image can be divided into three categories; type 1, distinct IS/OS line over central 2 mm; type 2, distinct IS/OS line only within central 2 mm; type 3, absent IS/OS line. *Red lines*: the length of the IS/OS line, which was detected on the gray-scale OCT image.

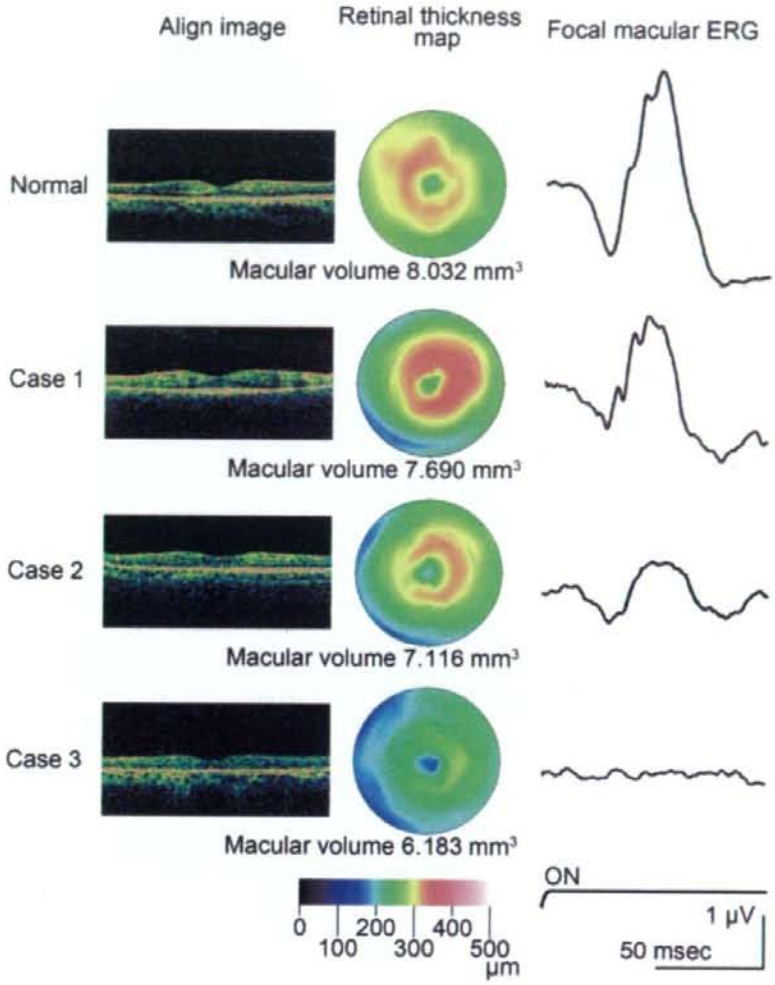


FIGURE 2. OCT images and fmERGs recorded from a normal subject and three representative patients with RP.

macular volume in patients with RP were significantly smaller than those of normal subjects ($P < 0.001$).

### Correlation between Amplitude of fmERG and Macular Volume

Because changes in the macular morphology should lead to functional changes,[52] we investigated whether there was a correlation between the amplitude of fmERGs and the total macular volume in our 43 patients with RP. The amplitudes of the a- and b-waves for 43 patients with RP are plotted against the total macular volume in Figures 4A and 4B, respectively. For both graphs, the gray area shows the 2.5 to 97.5 percentiles of normal control subjects.

A significant but weak correlation was found between the fmERG amplitude and total macular volume (a-wave, $\rho = 0.458$, $P < 0.01$; b-wave, $\rho = 0.540$, $P < 0.01$; Spearman's rank correlation). One of the reasons for this relatively weak correlation between the fmERG amplitude and total macular volume was that there were four patients with RP who had normal macular volume but severely reduced fmERG (e.g., patients 4–7, Fig. 4). In contrast, there were no patients with RP who had normal a- and b-wave amplitudes with severely reduced macular volume. There were two patients with RP who had normal a-wave amplitude with reduced macular volume, but their macular volumes were still near the lower borderline of normal, and their b-wave amplitudes were lower than the normal range.

### Correlation between fmERG and Length of IS/OS Line

We attempted to measure the thickness of each retinal layer (i.e., outer, middle, and inner retinal layers) separately, but found that it was very difficult to identify the border between these layers, especially in patients with relatively advanced stages of RP. The total macular volume is the sum of the volume of the neural retina in the central 6 mm of the retina and was used in the analyses. In addition, we used the length of the photoreceptor inner segment/outer segment junction

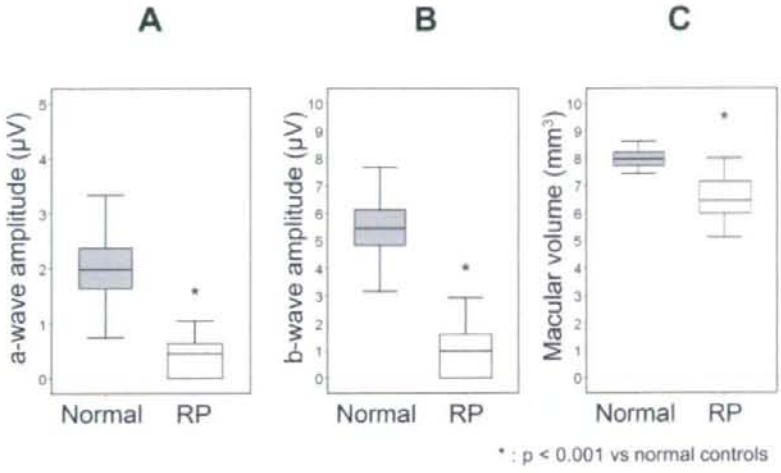


FIGURE 3. Box plots of the a- and b-waves of the fmERGs and total macular volume for normal controls and patients with RP. Line within the box indicates the median, the box the 25 and 75 percentiles, and the end of the error bars the 2.5 and 97.5 percentiles.

(IS/OS line) as a measure of the structural integrity of the macular area.

The amplitudes of the fmERG for the three RP groups classified by the length of the IS/OS line are shown in the upper traces of Figure 5 (see also Fig. 1). The amplitudes of the fmERGs in type 1 patients with RP (distinct IS/OS line over the central 2 mm) were significantly larger than those in type 2 (distinct IS/OS line only in the central 2 mm) and type 1 (absent IS/OS line) patients with RP ($P < 0.05$). Nine (81%) of 11 patients with type 3 RP had nonrecordable fmERGs, whereas none with type 1 had nonrecordable fmERGs (Fig. 5, bottom plot). These findings suggest that the patients with RP with longer IS/OS lines had larger fmERG amplitudes.

However, we found that the correlation between the amplitude of the fmERGs and changes in the OCT image was weak, even when the integrity of the IS/OS line was used to separate the patients with RP into the three groups. The weak correlation was probably due to two factors: first, there was no statistically significant difference in the fmERG amplitude between types 2 and 3 ($P = 0.07$ for a-wave; $P = 0.20$ for b-wave); and second, there was a large variation in the amplitudes of the fmERGs in type 1 and some patients had severely reduced amplitudes (Fig. 5, bottom plot).

### Patients with RP with Normal Macular Volume but Severely Reduced fmERGs

Finally, we wanted to investigate whether the IS/OS line was preserved in our four patients with normal macular volume and severely reduced fmERG amplitudes (Fig. 4). We expected that even though the total macular volume was within the normal range, these patients may have had a very short IS/OS line, which may be the reason for severely reduced mfERG. The gray-scale OCT images and the waveforms of fmERG in four patients with RP who had normal macular volume and severely reduced fmERG amplitude (patients 4–7) are shown

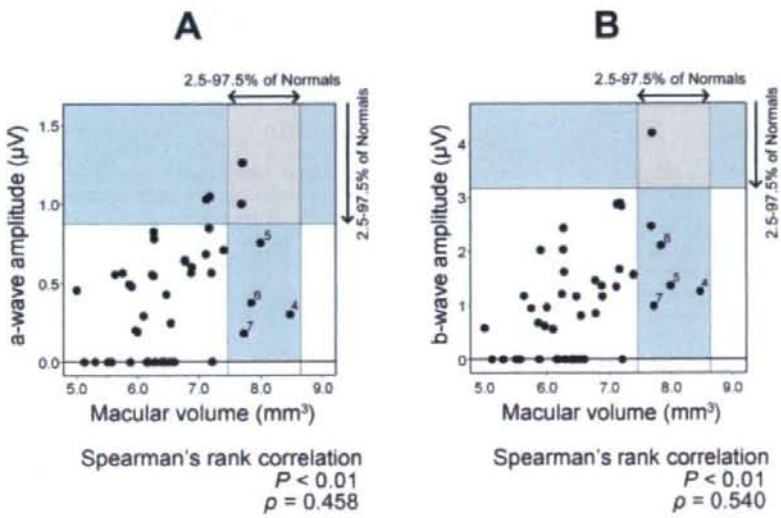


FIGURE 4. Amplitudes of a- and b-waves plotted against total macular volume in 43 patients with RP. There is a weak but significant correlation between the fmERG amplitude and total macular volume. There were four patients with RP who had normal macular volume but severely reduced fmERG (patients 4–7). *Shaded area*: the 2.5 to 97.5 percentiles of total macular volume and mfERG amplitude in age-similar normal subjects.